CERN Summer Student Report

Identification and space charge studies of offline ion sources in ISOLTRAP

Author:
N.M. Bouwman

Supervisors:
L. Nies
D. Lange
C. Schweiger

September 22, 2023

Abstract

With the offline laser ablation ion source that has recently been introduced to the ISOLTRAP experiment at CERN, carbon clusters can be produced and applied for relative and absolute precision mass measurements. The ablation products of three target materials (CuBe, Al, glassy carbon) placed in a new target holder were identified using time-of-flight mass spectrometry. With the carbon source, carbon clusters C_3^+ to C_{20}^+ were observed along with hydrocarbons at most mass numbers between $A = 36$ and $A = 84$. These hydrocarbons were determined to be largely produced by fragmentation of heavier clusters in collisions in the main buncher and appear to be abundant for $C_{2n}H_2^+$, $C_{2n}H_5^+$ and $C_{2n+1}H^+$. Furthermore, space charge effects in the MR-ToF MS were investigated for three isobaric pairs by examining peak shifts in the ToF spectra. In all cases, attraction between the isotope bunches was observed for increasing ion loads. The derived maximal ion flux in the MR-ToF MS at which the peaks become indistinguishable falls above the expected trend from simulations and earlier measurements.

Contents

1 Introduction

Determining the mass of exotic isotopes is crucial in nuclear physics to verify nuclear models, to expand knowledge of astrophysical nuclear processes and to investigate weak force interactions by beta decay. Radioactive isotopes are of particular interest due to their short lifetimes, which makes them challenging to contain and study. As part of the ISOLDE facility within CERN, the ISOLTRAP experiment conducts high level precision mass measurements of radionuclides [1]. This precision is achieved by combining a multi-reflection time-of-flight mass spectrometer (MR-ToF MS MS) with two Penning traps, although for very short-lived isotopes (less than 50 ms lifetime) the Penning traps are to be excluded due to their long trapping time. Additionally, the setup possesses a surface ion source and a new laser ablation ion source (LAIS) that provide ions for offline measurements, tuning of the setup and for precise mass references.

Prior to conducting mass measurements with the recently installed LAIS, it is crucial to identify the isotopes that it produces from several target materials. One reason for its introduction to the setup is that it can provide carbon clusters, which are molecules consisting of only carbon atoms. Laser ablation of a carbon sample has been shown to produce simple linear molecules such as C_3 and C_4 [2] up to fullerene molecules like C_{60} [3] and even molecules with up to 200 carbon atoms [4]. Firstly, these clusters have been proven useful for relative mass measurements due to the equidistant masses of the clusters, being a maximum of six mass units separated from any nuclide throughout the nuclear chart. Secondly, the clusters provide a method for absolute mass measurements [3], since the unit mass is closely related to that of ^{12}C. In this study, three target materials (CuBe, aluminium and glassy carbon) have been placed in a novel target holder for the LAIS source and the products have been analyzed with time-of-flight (ToF) spectra from the MR-ToF MS. Extra measurements have been conducted with the glassy carbon sample to investigate the properties of hydrocarbons formed from the carbon clusters in the ISOLTRAP buncher.

Recent simulations have demonstrated the influence of space charge effects in MR-ToF MS devices on the observed separation of isotope bunches [5]. It has been shown that the ToFs of two isotope bunches attract due to Coulomb effects when the number of ions in the MR-ToF MS is increased. This becomes more significant in case of a small mass difference or initial time spread, causing two peaks to coalesce completely. Especially when contaminations are more abundant than the isotope of interest, it is essential to determine how many ions are permitted in the MR-ToF MS per shot to keep the peaks distinguishable. In the second part of this study, space-charge effects in the MR-ToF MS between three isobaric pairs from the ISOLDE beamline have been investigated for a range of ion densities.

2 Experimental setup

A schematic drawing of the ISOLTRAP setup is shown in Figure 1. The setup can either receive a radioactive ion beam from the ISOLDE central beamline or produce its own ions by means of a surface ion source or a laser ablation ion source (LAIS). A beam of ionized isotopes first enters the main buncher, where an electric potential well is provided by four rows of electrodes along the length of the trap [6]. The ions are radially confined by radiofrequency (RF) electric fields arising from oscillating voltages on the same electrodes and are thermalized by means of collisions with a helium buffer gas at ambient temperature (300K) [7]. After a cooling time of typically 10 ms, the bunches are ejected at 30 keV energy into a pulsed drift tube, of which the potential

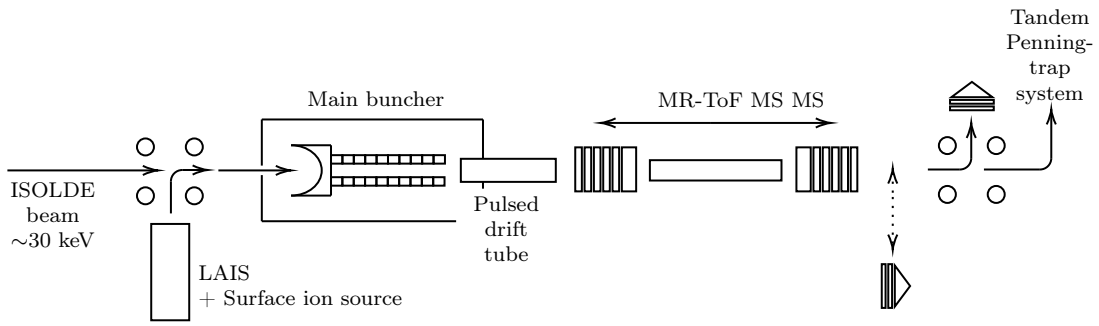

Figure 1: Schematic drawing of the horizontal section of the ISOLTRAP setup. The Penning traps have been omitted for the purpose of this research.

is switched from 26.8 kV to 0 V to reduce the kinetic energy of the bunch to only 3.2 kV [8]. Due to the slight differences in velocity between ions of different masses, the exact timing of this voltage switch selects a mass range that can be analyzed in the setup. Given enough distance, even isotopes with arbitrarily small mass differences will separate in space. This time-of-flight separation is performed in the MR-ToF MS, of which the cavity voltage is lowered to reflect the charged particles between its two electrostatic mirrors on either end [9]. Raising the voltage again after a selected number of revolutions allows only the ions travelling in the downstream direction to leave the MR-ToF MS towards the subsequent ion traps. The arrival time of the separated isotope bunches can then be measured either by a moveable electron multiplier (EMP) particle detector in the beamline or by one placed perpendicular to it. Alternatively, they can be sent towards the double Penning trap system for further separation and measurements. In this case, the ions first undergo mass selective buffer gas cooling in the preparation trap [10]. Once the ions of interest have gathered in the centre, they are injected into the precision trap, in which their masses can be measured using either the time-of-flight ion-cyclotron-resonance (ToF-ICR) [11] or phase-imaging ion-cyclotron-resonance (PI-ICR) [12] techniques. In these methods, the mass-over-charge ratio of the isotope of interest is measured respectively by its ToF out of the Penning trap or by the phase of its orbit in the Penning trap. The combination of the MR-ToF MS and the Penning traps reaches relative mass precision values up to 10^{-10}, depending on the ion's absolute mass and storage time in the traps. If for short-lived isotopes the MR-ToF MS is to be used on its own, a relative mass precision up to around 10^{-7} can be reached.

The two ion sources in front of the buncher provide ions in offline settings. The surface ion source produces predominantly the alkali ions $^{39}K^+$, $^{85,87}Rb^+$ and $^{133}Cs^+$, which are stored in a zeolite sample and evaporate when the material is heated [1]. In the LAIS, a 523 nm Nd:YAG laser is shone from above onto a movable target with nanosecond pulses, forming a plasma on the surface of the sample in the exposed area. A laser energy in the order of µJ is enough to eject ions into the environment, which are extracted using electrostatic lenses and merged with the main beamline.

3 Theory

The bunches leaving the pulsed drift tube comprise ions in a range of masses. Since they are ejected at similar energies, the kinetic energy of the lighter isotopes will be larger than that of the heavy ones. Different masses can be completely separated by their time of flight with appropriate

travel distance, which is attained by reflecting the ions in the MR-ToF MS. The mass resolving power of 300k as achieved with this device allows even for the distinction between isobars and certain isomers.

Many parameters of the experimental setup influence the ToF of an isotope, including the length of the MR-ToF MS, the strength of the electrostatic mirrors and the amount of revolutions inside the MR-ToF MS. If these effects are compacted into parameters a and b, the time of flight can be expressed as

$$t = a\sqrt{\frac{m}{q}} + b, \tag{1}$$

where m/q is the mass-over-charge ratio of the isotope [9]. For a fixed number of revolutions, the two parameters are constant and hence the ToF of different masses travelling through the setup under the same conditions only depends on m/q. Values for a and b can be computed if the ToF of two well-known isotopes is determined, acting as a calibration for masses in the same range to be investigated. The systematic errors in a mass measurement therefore increase when the mass of interest is far separated from those used for the calibration.

An isotope bunch appears as a peak in the ToF spectrum as measured by one of the detectors. Since the ions are thermalized in the buncher, they are expected to follow Boltzmann statistics, giving rise to a Gaussian distribution of the velocities within each species [13]. However, the ToF peak shape is adjusted due to the ion acceleration during ejection and due to fluctuations in experienced electric field in the MR-ToF MS, as well as collisions of the ions with atoms in the environment. The observed peaks are fitted with the hyper-EMG function, which describes a Gaussian with a given amount of additional exponentially decaying tails to the left and to the right [13].

For different ion loads in the MR-ToF MS, the peaks in the spectrum shift due to space charge effects. It is known that when the amount of positive charges in the MR-ToF MS is increased, ions with similar masses counter-intuitively attract and match their ToF. This leads to coalescence of peaks of different isotopes, but also to self-bunching within a single species [14]. A ground theoretical explanation of this concept has not yet been provided, but it is hypothesized that the attraction is mainly caused by Coulomb repulsion during reflection in the electrostatic mirrors, depending on the shape of the electrostatic potential. [14]. Indeed, if an isotope bunch has been reflected in its turning point and is met shortly after by a higher mass, then the mutual repulsion might decrease the acceleration of the former and increase the deceleration of the latter, shifting the ToFs closer together. The maximal ion count N_{max} is defined as the number of ions in the MR-ToF MS at which two peaks of interest overlap such that 7% of either of the peaks is obscured by the other [5]. The maximal ion flux is then expressed as

$$\phi = \frac{N_{max}}{t_s}, \tag{2}$$

where t_s is the storage time in the MR-ToF MS, which is close to the total ToF if it is measured from insertion into the MR-ToF MS device onwards. This flux has been show to have a strong inversely exponential relation to the $m/\Delta m$ ratio of the peaks [5], commonly written as $m_1/(m_2 - m_1)$ where m_1 and m_2 correspond to the lighter and heavier isotope respectively.

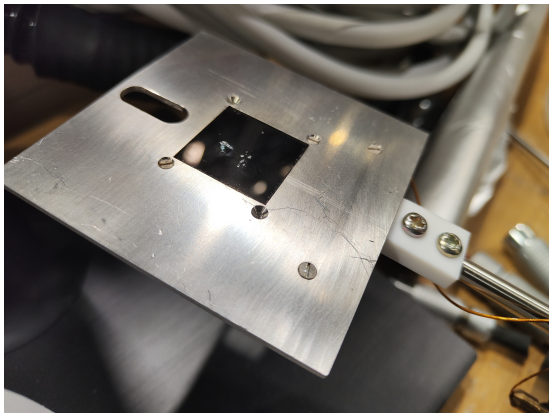

Figure 2: Original target holder for the LAIS, holding an ablated carbon sample.

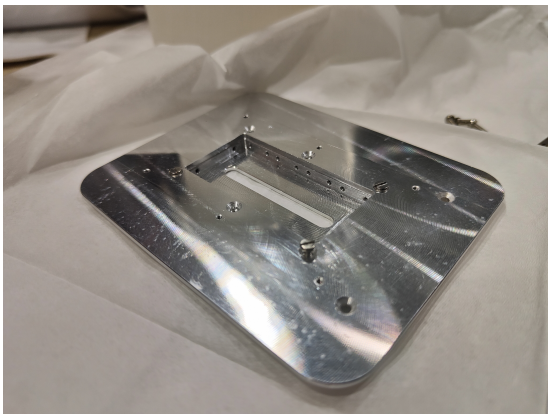

Figure 3: New LAIS target holder, capable of holding two square 1 inch samples or multiple smaller ones.

4 LAIS source identification

4.1 Target holder design

In preparation of the LAIS target studies, a new target holder was designed in the CAD software *Autodesk Inventor* to contain multiple laser ablation targets and was manufactured and assembled at CERN. The holder can be moved 50 mm horizontally by a small motor, enabling the laser to hit different materials. Figures 2 and 3 show the original and current target holders respectively. In Figure 4, a render of the CAD model is displayed with a small target inserted in the cavity.

4.2 Identification of LAIS targets

Three target materials were placed onto the target holder during its installation: a thin CuBe sheet, a block of aluminium and a glassy carbon sample. The laser was focused on the three samples successively and ToF spectra were acquired using shoot-through measurements in the MR-ToF MS. Figure 5 displays the obtained spectrum for the CuBe target, along with the names of several molecules that are expected to correspond to the peaks. Whereas most peaks only contain several counts, the peak located at the ToF of $Be_3{}^+$ reaches significantly higher, which suggests that this molecule is predominantly produced in the target and could be the most stable beryllium cluster. However, it is worth noting that shorter ToFs are not visible due to the pulsed drift tube timing being tuned to ^{39}K at the lowest. The two following largest peaks might correspond to $CBe_3{}^+$ or K^+ and $CuBe_2{}^+$. Furthermore, small hints towards the presence of heavy beryllium clusters such as $Be_{11}{}^+$ and $Be_{12}{}^+$ are noticed.

For the aluminium sample, no clear peaks were seen in the considered ToF range. The ToF spectrum in Figure 6 shows one bin that might correspond to the cluster $Al_5{}^+$, but more statistics are needed to properly identify any molecules.

The glassy carbon target provides a more insightful spectrum. In the spectrum shown in Figure 7, a variety of peaks is seen with regular spacing in between. Using the ToFs of $^{39}K^+$ and $^{85}Rb^+$ from the alkali source as calibration, the predicted ToFs of carbon clusters align with the observed peaks from the LAIS, suggesting that at least the clusters $C_3{}^+$ up to $C_{20}{}^+$ are produced in the laser ablation source. A clear abundance of $C_{10}{}^+$, $C_{11}{}^+$ and $C_{15}{}^+$ is seen in

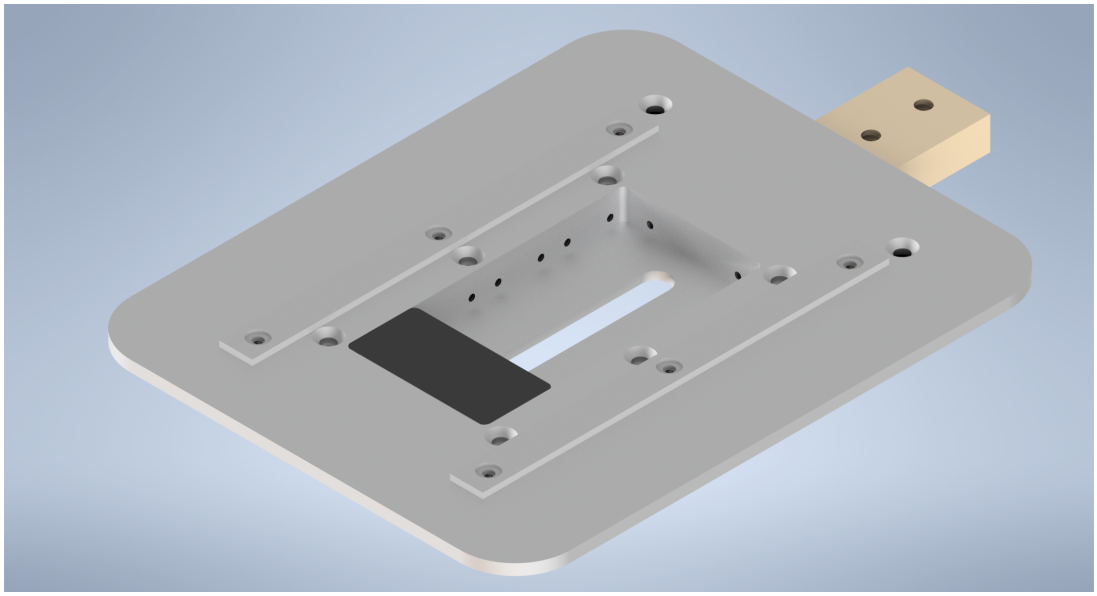

Figure 4: Rendered CAD model of the improved LAIS target holder holding one 0.5x1 inch sample.

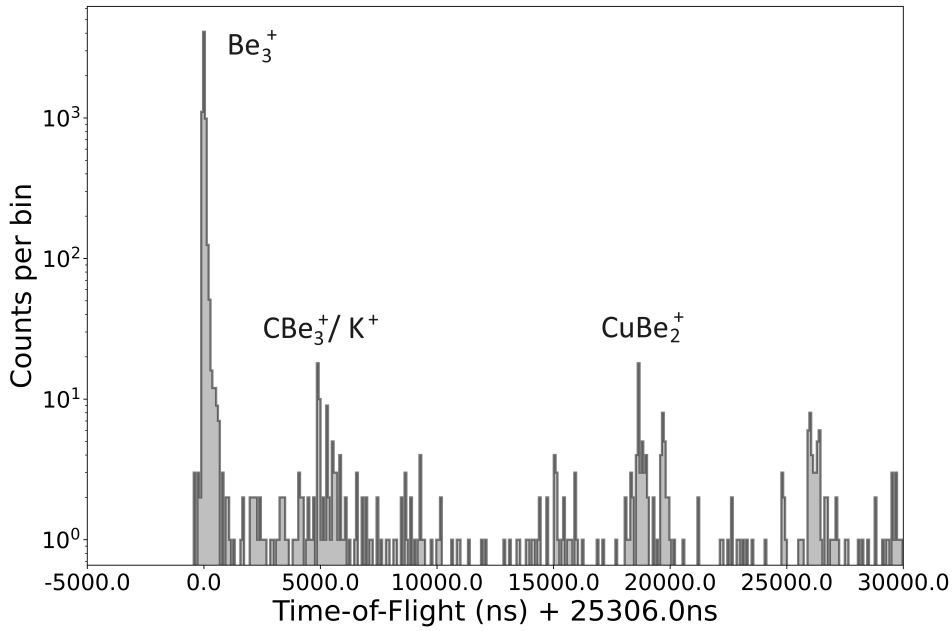

Figure 5: ToF spectrum obtained by ablating a CuBe target in the LAIS. Several molecules have been suggested for the peaks, of which the predicted ToFs are indicated by vertical dotted lines.

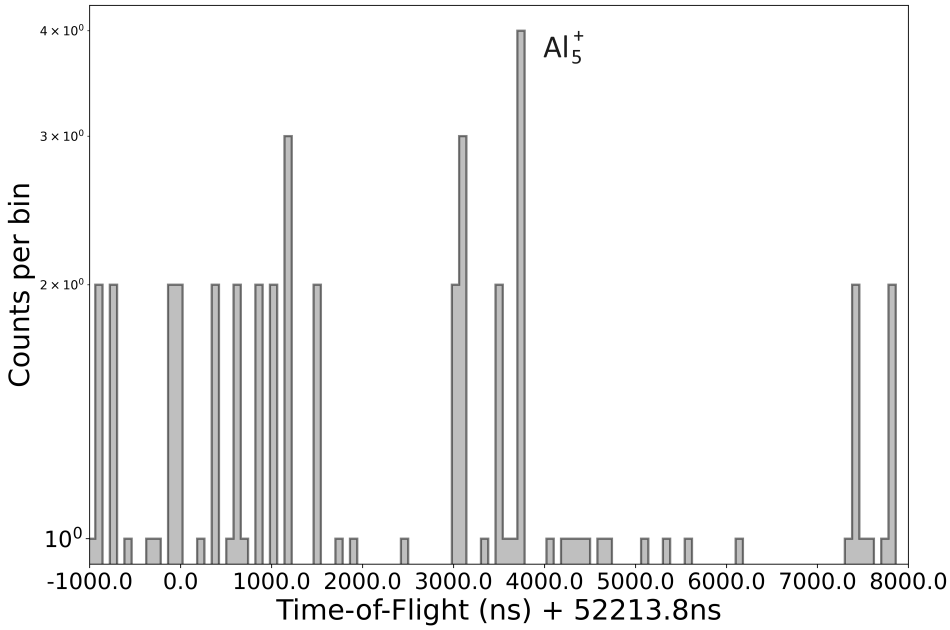

Figure 6: ToF spectrum obtained by ablating an aluminium target in the LAIS. The predicted ToFs of some aluminium based molecules are indicated by vertical dotted lines.

particular, along with a similar pattern between $C_{10}{}^+$-$C_{13}{}^+$ and $C_{14}{}^+$-$C_{17}{}^+$. These observations suggest a similar structure of the carbon clusters in this range and support older findings [2], [15], [16]. Moreover, the high peaks of smaller masses are noticed to be offset from the carbon cluster masses. This range of the spectrum is analyzed in detail in the rest of this section.

4.3 Analysis of hydrocarbons

Small carbon clusters are mainly represented by linear molecules. These are either cumulenes $\cdots C = C = C \cdots$ with a double bond between each carbon atom or polyynes $\cdots C - C \equiv C \cdots$ which contain alternating single and triple bonds [15]. The free ends of these molecules can bind with hydrogen atoms to form hydrocarbons. Cumulenes are able to bind up to two H atoms at each end, whereas polyynes can either bind with one or three hydrogen atoms on either end depending on the type of bond between the penultimate carbon atoms. Fewer H bonds are allowed but create radicals, which would react shortly after forming. This allows up to 6 hydrogen atoms to be added to the carbon clusters and predicts a preference for C_nH_2, C_nH_4 and C_nH_6.

The mass range between $C_3{}^+$ and $C_7{}^+$ from the spectrum in Figure 7 is shown in detail in Figure 8. Besides the carbon cluster peaks separated by regular intervals, the spectrum reveals many other peaks accompanying the clusters. Exactly 11 peaks are counted between $C_3{}^+$ and $C_4{}^+$, implying that molecules of every mass number in this range are produced in the setup. The simplest explanation for these molecules are the aforementioned hydrocarbons that could be produced from the linear carbon clusters. The six peaks after each cluster are indeed abundant in most cases, although larger molecules appear as well. For the even carbon clusters, a clear preference for the molecules $C_{2n}H_2{}^+$ and $C_{2n}H_5{}^+$ is observed, while for the odd clusters only the $C_{2n+1}H^+$ peak protrudes.

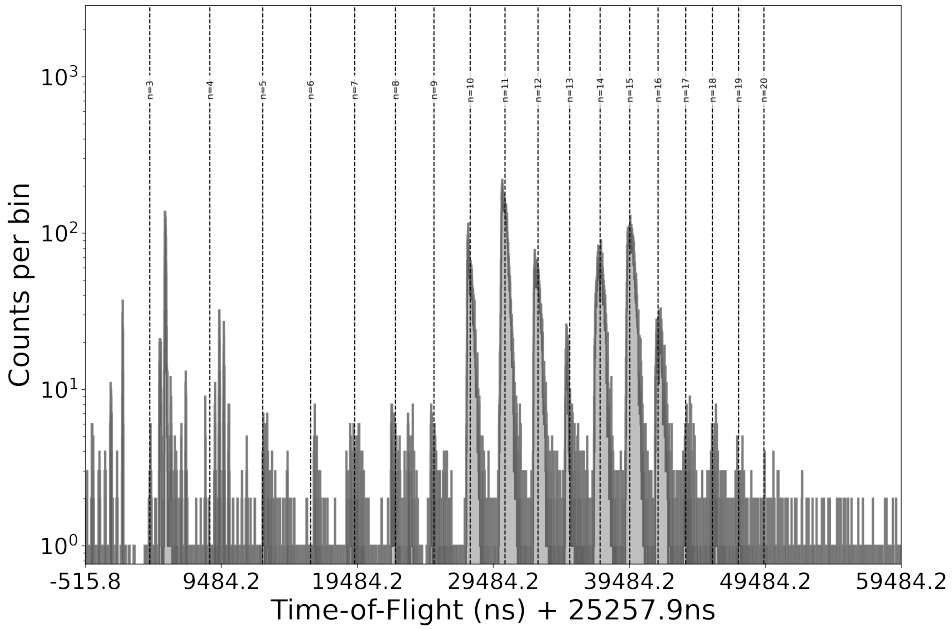

Figure 7: ToF spectrum obtained by ablating a glassy carbon target in the LAIS. The predicted ToFs of all carbon clusters $C_n{}^+$ with n between 3 and 20 are indicated by vertical dotted lines.

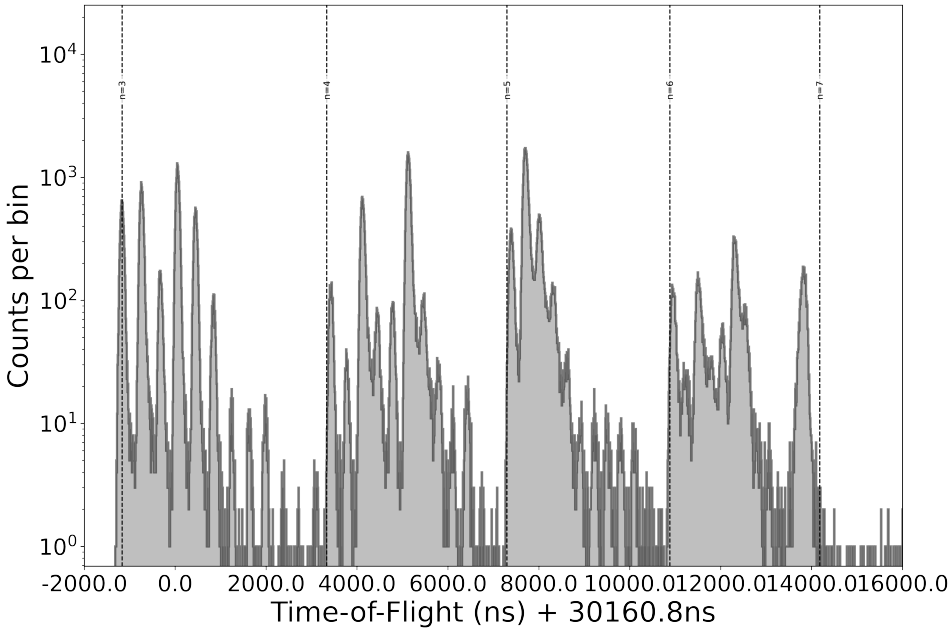

Figure 8: Low mass region of the ToF spectrum obtained by ablating a glassy carbon target in the LAIS. The predicted ToFs of the carbon clusters $C_n{}^+$ with n between 3 and 7 are indicated by vertical dotted lines.

In order to determine where in the setup the molecules are produced, a scan was performed where the cooling time in the main buncher was increased from 4 ms up to 50 ms in steps of 2 ms. The spectrum on top is a copy of that in Figure 8, except now similar molecules are given the same colour and only the first six molecules corresponding to each cluster are displayed. The teal peaks correspond to the carbon clusters $C_n{}^+$ of mass number $12n$, the lime peaks to the hydrocarbons C_nH^+ with mass numbers $12n + 1$, and so forth. The bottom graph shows the relation between the number of counts of each type of molecule compared to that at a cooling time of 4 ms. While the number of carbon clusters is seen to decrease immediately, many of the hydrocarbons stay more stable in count before the amount drops. For $C_nH_3{}^+$ in particular, the relative amount of counts increases up to around 1.4 at 10 ms cooling time. These results suggest that many of the detected molecules are formed in the buncher, because the hydrocarbon count does not decrease as rapidly as that of the carbon clusters. This could either be due to carbon clusters $C_n{}^+$ attaching to hydrogen in the environment to form $C_nH_m{}^+$ or due to fragmentation of larger clusters by collisions with other molecules. For higher cooling times, all the peaks reduce significantly.

To investigate the origin of the hydrocarbons more precisely, the total counts in each group of peaks corresponding to one carbon cluster (masses $12n$ up to and including $12n+11$) were added up and compared using the same data set. Figure 10 shows how the counts in each group for n between 3 and 7 change with increasing cooling times, along with the carbon cluster counts in grey. The groups are all observed to decrease in count slower than the carbon clusters. Whereas the number of counts in the heaviest hydrocarbon group drops immediately, the lightest group is noticed to start diminishing the latest at around 10 ms cooling time, while the relative counts of the middle two groups fall between these two extremes over the entire range. This suggests that the detected hydrocarbons are mostly produced by collisions in the main buncher, as the heavier groups could split up into hydrocarbons with $n = 3$, keeping the count stable for longer cooling times.

5 Peak coalescence in the MR-ToF MS

Although the obtained ToF spectra suffice for the mere identification of peaks, the derived mass over charge ratios might be off due to space charge effects in the MR-ToF MS device. Since ISOLTRAP studies rare radionuclides, peak coalescence becomes problematic when contaminations are present in high amounts or have a similar mass to that of the isotope of interest. The peak coalescence effect in the MR-ToF MS was investigated for three isobaric pairs produced in a ThC VD5 target from ISOLDE: SmF^+ and NdF^+ (mass number $A = 167$), $SmF_2{}^+$ and $NdF_2{}^+$ ($A = 186$) and the isobars Ra^+ and Fr^+ ($A = 225$). These pairs have $(m_2 - m_1)/m_1$ ratios of 80642, 89821 and 114693 respectively.

5.1 ToF attraction between isobars

The space charge effects were investigated by performing beamgate scans, in which the duration of open beamgate was varied to allow different amounts of ions into the main buncher. A separate scan was taken for each isobaric pair and the datafiles were divided into shots with equal multiplicity, a measure that represents the amount of ions observed by the detector during a single shot. A hyper-EMG function with two right tails was fitted to the peaks in the spectrum for each multiplicity.

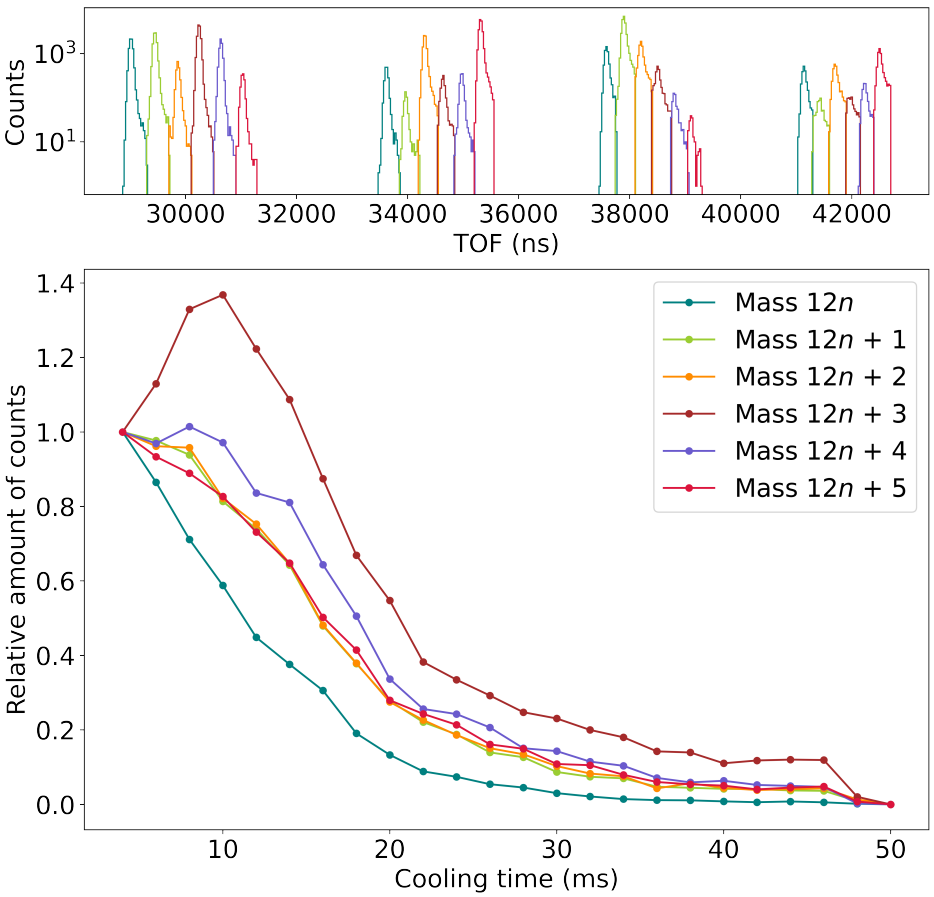

Figure 9: Relation between the sum of counts over similar hydrocarbons relative to that of the first measurement and the cooling time in the main buncher, where similar hydrocarbons have an equal amount of H atoms. The ToF spectrum on top shows the peaks of the six considered molecule types $C_n{}^+$ to $C_nH_5{}^+$ with n ranging from 3 to 6.

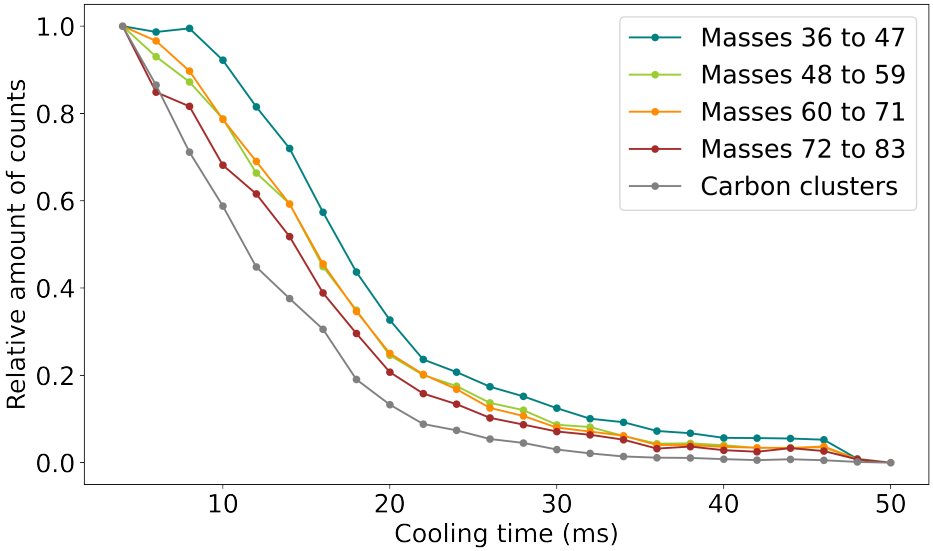

Figure 10: Sum of counts over the eleven hydrocarbon peaks corresponding to each carbon cluster, relative to the first measurement, against the cooling time in the main buncher. The relative amount of counts for the carbon clusters from Figure 9 is shown in grey as comparison.

To illustrate the fitting procedure, Figure 11 shows the evolution of the ToF spectrum of the Ra^+, Fr^+ pair for multiplicities 5, 22 and 49, along with the best fit of two hyper-EMG functions. The peaks start out decently separated and the statistics increase when the multiplicity is increased. However, for 49 detected ions per shot, the two peaks appear broader and overlap considerably, making it more difficult to extract the peak positions. The peaks are seen to attract, as expected from the coalescence effect.

This shifting of the peaks is more noticeable in Figure 12, in which the peak positions are plotted against the multiplicity for all three pairs. A linear function has been fitted through the data points by means of weighted linear regression, where the weights correspond to the reciprocal of the uncertainty in the peak centres. For the lightest pairs, both bunches are observed to shift up in ToF but appear to approach one another, whereas for the heaviest pair the two peaks attract directly. Figure 13 shows the peak separation, along with a linear regression fit and its reduced χ^2 value, for which the degrees of freedom is equal to $N-2$ where N equals the amount of data points. In all three cases, the ToF difference decreases linearly in the considered range, clearly reflecting the peak coalescence due to space charge effects.

With the standard deviation σ of the peak fit, the multiplicity at which the peaks become indistinguishable can be estimated. A simplified assumption to be made is that the two peaks are Gaussian and of equal height. In this case, both peaks overlap for 7% when their intersection line, which lies exactly in the middle of the two peaks, equals the z-value that covers 3.5% of the area of one peak. This occurs at around 1.8σ from the center of the peak. Thus, when the peak positions are approximately 3.6σ separated, the peaks are said to be inseparable. For the three isobaric pairs in the previously listed order, the standard deviations are around 55 ns, 68 ns and 72 ns respectively. Extrapolating the linear fits, the overlap is found to occur at multiplicities 367 ions/shot, 97 ions/shot and 52 ions/shot corresponding to a flux of approximately 5900 ions/s,

1600 ions/s and 700 ions/s in the MR-ToF MS. These values are compared to similations and previous measurements with other MR-ToF MS devices in Figure 14, which has been adapted from a recent study of MIRACLS on peak coalescence in MR-ToF MS devices [5]. The obtained data points appear to be higher than the visible trend in the simulations but are less than an order of magnitude off. A similar offset is seen in the other low $\Delta m/m$ data point corresponding to earlier ISOLTRAP measurements. However, since ions are lost in the MR-ToF MS due to collisions with the residual gas, the actual flux in the device is expected to be above the ones derived in this study, which would create a larger offset than shown in the plot.

5.2 Beamgate and multiplicity

It is important to realize that the flux at which the peak coalesce was obtained by scanning over the amount of ions detected after they pass through the setup. However, the variable that is controlled is the beamgate, which might not correspond linearly to the multiplicity due to ion losses in the buncher and the MR-ToF MS through collisions with the environment. For the dataset of $SmF_2{}^+$ and $NdF_2{}^+$, the distribution of multiplicities was plotted for beamgates between 20 ns and 100 ns in steps of 20 ns. The distributions were fitted with Gaussian functions. Figure 15 shows that the distribution of multiplicities spreads out when the beamgate is increased. This indicates that low multiplicities mainly correpond to low beamgates, but higher multiplicities can be caused by a growing range of beamgate values. Hence, the peak overlap of 7% might occur at a lower beamgate than expected due to the large spread of resulting ions counts in the MR-ToF MS. However, as seen in Figure 16, the average multiplicity still appears to increase linearly.

6 Discussion

6.1 Al and CuBe spectra

Because the obtained ToF spectra by laser ablation of the aluminium and CuBe targets yielded poor statistics, identification of the products was challenging. Reasons for the low number of counts might be the energy of the laser and its focus area on the materials. Both increasing the energy and reducing the area hit by the laser could contribute to raising the energy transfer to the material and may lead to a greater production of ions. Moreover, since the aluminium sample is known to be reflective, it might be necessary to first destroy and roughen its surface by repeated ablation to produce the aluminium cluster production. For both materials it is worth conducting shoot-through measurements with a lower selected mass range in order to examine the low mass region of the spectrum. Once statistics are increased, revolving the ions in the MR-ToF MS would reveal the composition of the molecules and clusters and may open up their use for calibrations and tests of the ISOLTRAP experimental setup.

6.2 Hydrocarbon identification

The ablation of the glassy carbon source provided carbon clusters between $C_3{}^+$ and $C_{20}{}^+$, of which the production was found to depend strongly on the laser energy. Clusters below and above this range might also be created from the target and could be detected by selecting different mass ranges in the pulsed drift tube or by varying the disposed energy. Nonetheless, the obtained clusters enable precise absolute mass measurements of nuclides with any mass number between

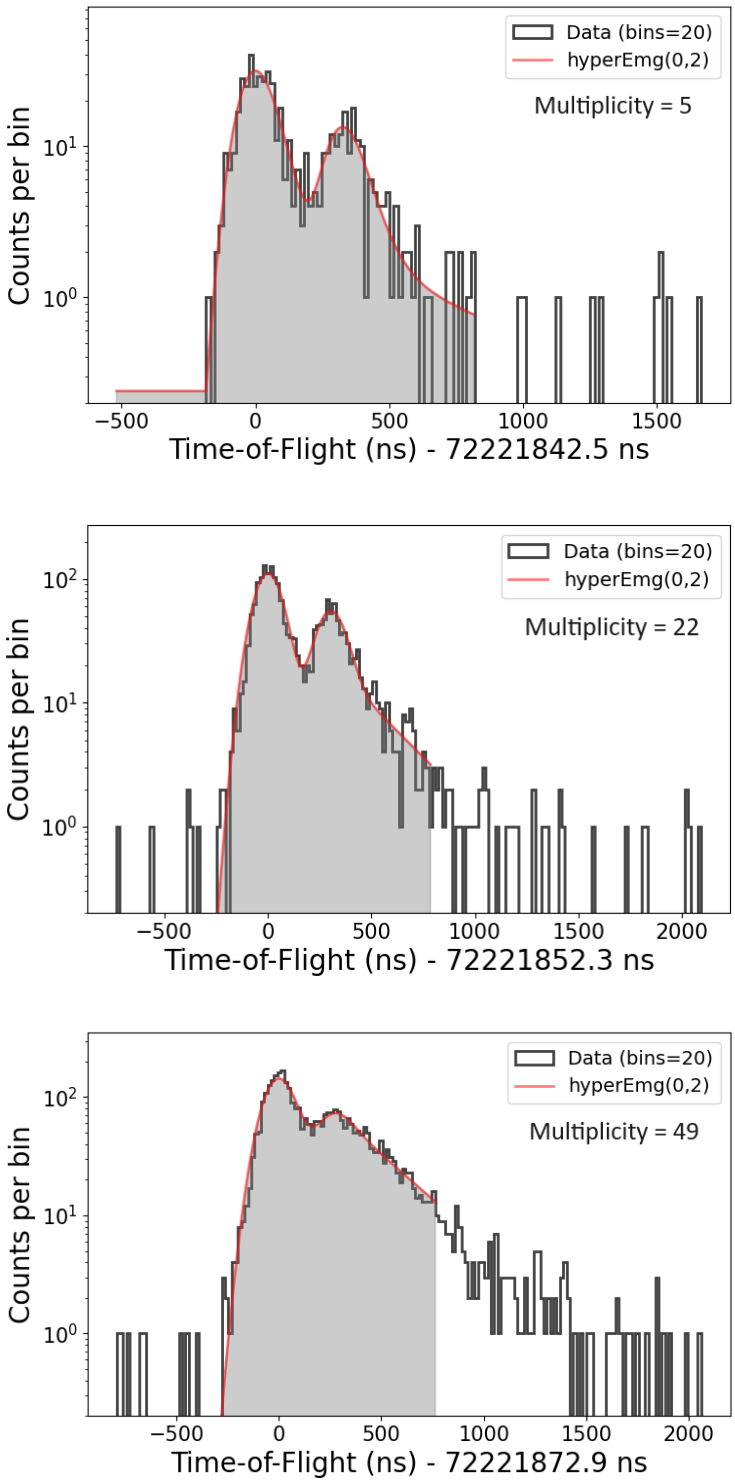

Figure 11: ToF spectra of shoot-through measurements for Ra^+ and Fr^+ at mass number $A = 225$, showing the peak shapes resulting from shots at different multiplicities. Two hyper-EMG functions with two right tails are fitted through the peaks to determine the peak positions.

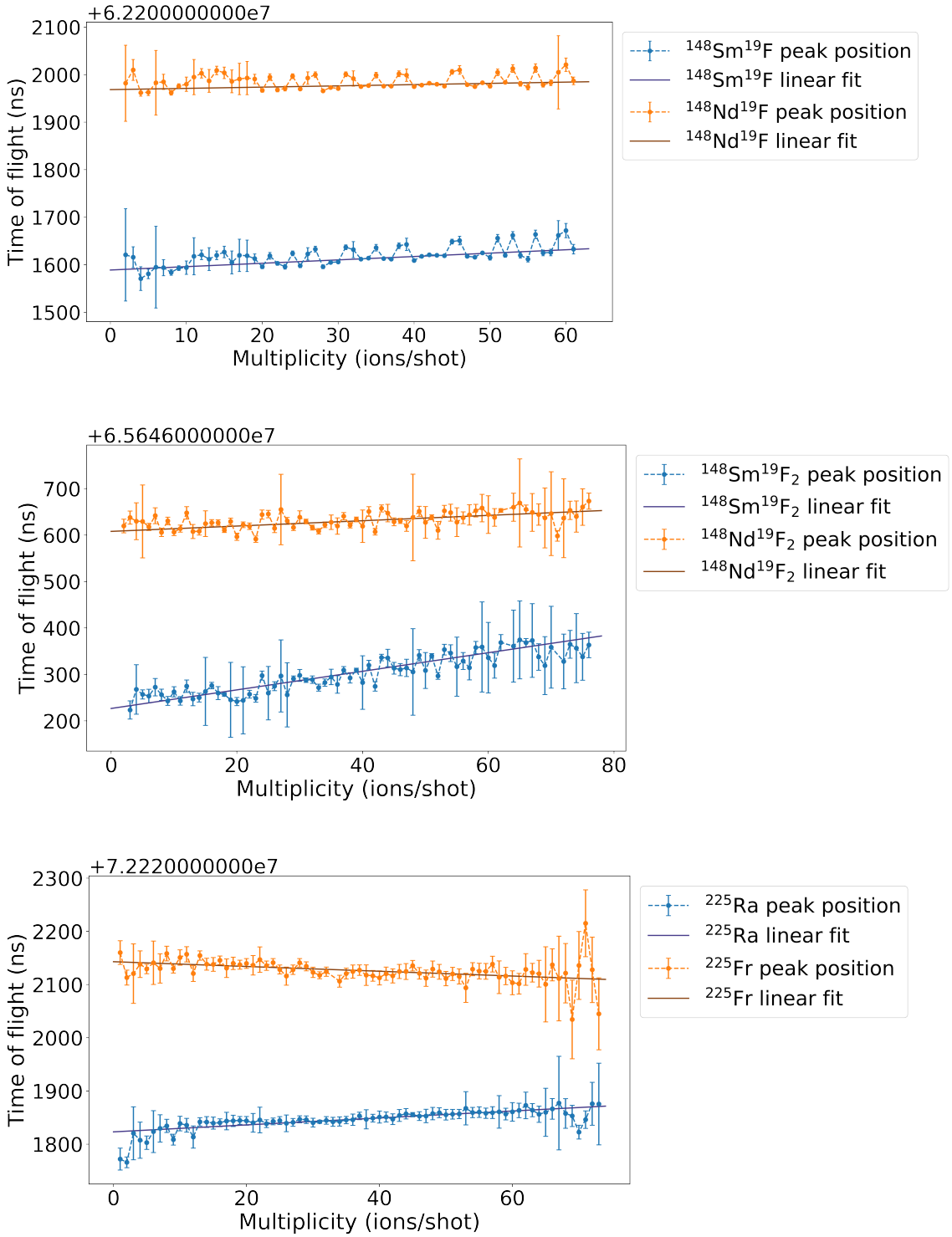

Figure 12: ToFs of the peak positions of the three isobaric pairs against the multiplicity as measured by the detector. The peak positions with their error bars have been extracted from the centers of the hyper-EMG fits and their uncertainties. Linear fits through the data points have been contructed by linear regression and show the overall attraction of the peaks.

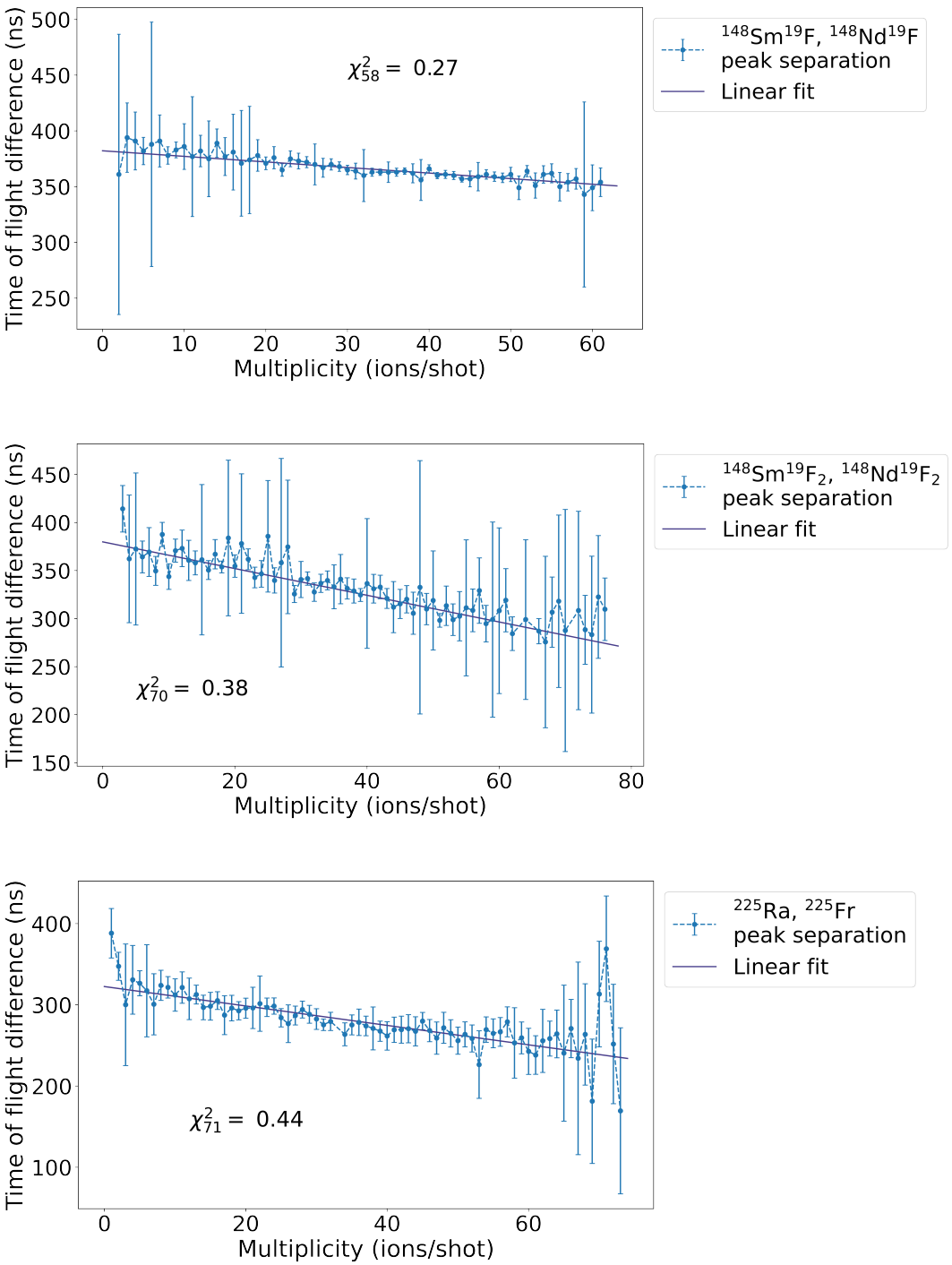

Figure 13: ToF separation between the peak positions of the three isobaric pairs from Figure 12 against the multiplicity as measured by the detector.

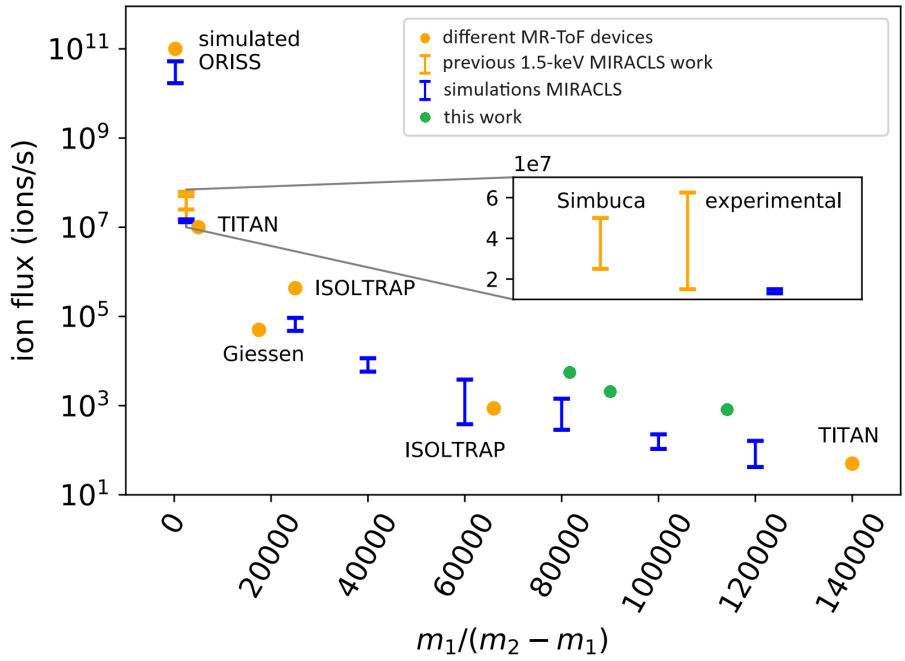

Figure 14: Comparison of the maximal ion flux versus $\Delta m/m$ between the results obtained in this work, simulations from MIRACLS and experimental values found by several MR-ToF MS devices. The latter includes earlier results from ISOLTRAP in which more than 7% overlap is observed, which is a potential explanation for the high offset. A similar offset is seen in the results from this work. Figure adapted from MIRACLS study [5].

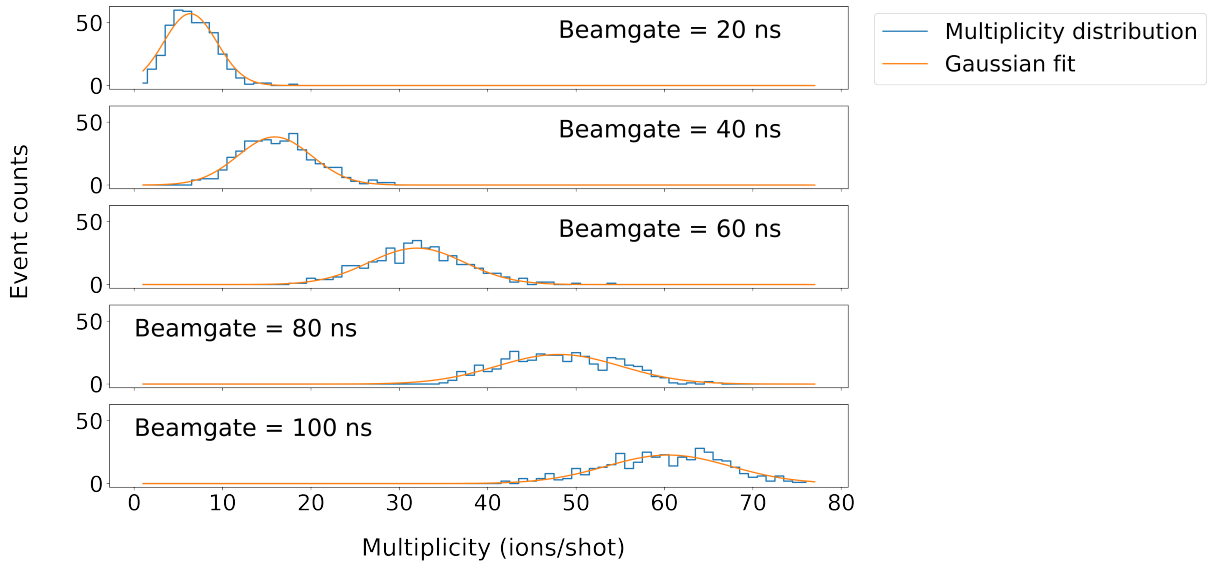

Figure 15: Distribution of multiplicities observed by the detector for five beamgame values. Gaussian functions have been fit through the data.

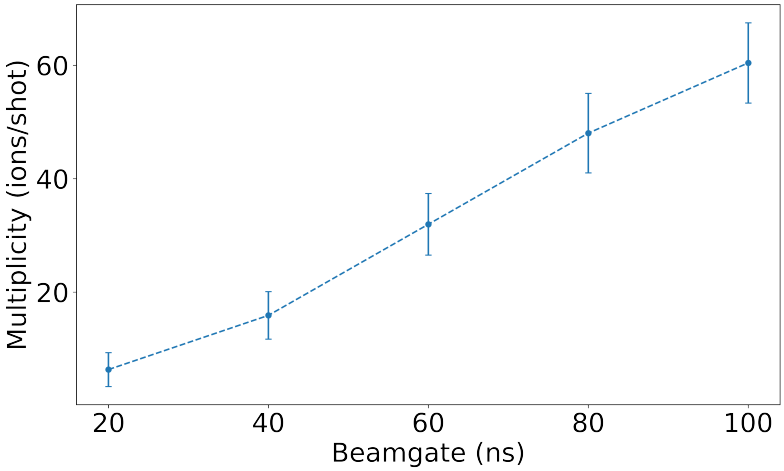

Figure 16: Relation between the extracted mean of the Gaussian fit through the multiplicity distribution against the beamgate value. The error bars correspond to one standard deviation of the fits.

$A = 36$ and $A = 240$ due to the regular spacing between the clusters. Although the clusters $C_{10}{}^{+}$ and upwards were produced significantly, the peaks in the spectrum showed a broad right tail. This might be caused by the formation of hydrocarbons in the main buncher or by the presence of ^{13}C atoms between the far more common ^{12}C, which is expected since graphite contains 1.1% ^{13}C [16]. As a result, the peaks in this range might be close enough in ToF to overlap, as the ToF of isotopes scales with the square root of its mass-over-charge ratio. To investigate the separability of these heavy molcules, extra measurements could be conducted that implement multiple revolutions of the clusters in the MR-ToF MS.

Similar measurements can be carried out for the lighter hydrocarbons to determine precisely what molecules or atoms the observed peaks correspond to. They have been assumed to be represented by linear hydrocarbons, although more complex molecules are required to explain peaks in the higher region of the $C_3{}^{+}$ hydrocarbon group. Instead of binding only to the free ends of the linear molecules, collisions between molecules in the setup might break double or triple bonds between the carbon atoms and allow hydrogen to bind with any carbon atom in the molecule. This method can produce propane ions ($C_3H_8{}^{+}$) which would explain the peak at mass $A = 44$. Alternatively, oxygen from the environment could bind and form oxides, which has been shown to occur significantly in the buncher [17]. Indeed, a peak at mass number $A = 47$ is noticed despite $C_3H_{11}{}^{+}$ not being allowed due to the limited amount of available bonds. It might correspond to $CO_2H_3{}^{+}$ if the absence of any other nuclides is assumed, which would make the molecule a radical. Cyclic carbon clusters might be present as well and could add to the count of light hydrocarbons.

It is yet unclear why $C_{2n}H_2{}^{+}$ and $C_{2n}H_5{}^{+}$ seem to be preferred for even clusters and $C_{2n+1}H^{+}$ for odd clusters. Similarly, what appears to be C_6H_{11} is very abundant compared to the neighboring molecules. It might conversely correspond to C_7, although this would change the interpretation of the other molecules due to a calibration shift. Such a shift might in turn explain the former abundances if the peaks are now caused by $C_{2n}H_3{}^{+}$, $C_{2n}H_6{}^{+}$ and $C_{2n+1}H_2{}^{+}$ which are expected for the given carbon clusters, yet would greatly diminish the carbon cluster count. It is

therefore essential to separate and identify the molecules by increasing their ToF in the MR-ToF MS.

6.3 Peak coalescence

The plots in Figure 13, displaying the relation between multiplicities and peak positions for the three isobaric pairs, all show a steady decrease, which clearly demonstrates the attraction between the isotope bunches due to space charge effects in the MR-ToF MS. However, the absolute position of the peaks as shown in Figure 12 appears to shift up and down in a seemingly random manner. This is especially noticeable for SmF^+ and NdF^+, for which the data points show similar fluctuations around the linear fit. Shifts in the entire ToF spectrum might be caused by fluctuations in temperature in the environment or by disturbances in the electric fields from the lenses. Nonetheless, this does not explain the ToF shifts of more than 30 ns between consecutive multiplicities, as only five beamgate values were selected and gave rise to an approximately Gaussian distribution of multiplicities each. A similar behavior is seen in the case of $SmF_2{}^+$ and $NdF_2{}^+$, for example around a multiplicity of 40, although the effect is less clear. Although this common shift is filtered out when the separation between the peaks is considered and does therefore not influence the final results, it requires a more detailed investigation.

The distance between the peaks appears to decrease linearly in the covered multiplicity range. However, the reduced χ^2 value is low in all cases, which might indicate that a horizontal line fits the data better. Regardless, it is argued that a significant lowering of the ToF difference is noticed and that the high value of χ^2 could be due to the large error in several fits. The size of the error bars might be caused by limited statistics for a given multiplicity, which occurs not only for very low multiplicities due to the few obtained ToFs but also for very high multiplicies due to the small amount of events producing bunches of this many ions. This increases the uncertainty in the mean position of the peaks. To improve statistics for low multiplicities, longer measurements with shorter beamgates may be conducted. The high end is more difficult to reach, as the detector saturates if too many ions hit the surface in a single shot. This effect is observed as a broadening of the peak on the right side, which could increase the uncertainty in peak position as well.

The maximal ion flux values derived from the measured peak shift are higher than expected from simulations and experimental work from other MR-ToF MS devices, as noticed in Figure 14. Moreover, realistic flux values will increase further when ion losses in the MR-ToF MS is considered. A reason for this offset might be the simplicity of the assumptions made to determine the multiplicity at which the peaks become indistinguishable. One of the assumptions is that the peaks are represented by perfect Gaussian functions, although they were accurately fitted by the hyper-EMG function with two tails earlier in this work. This right tail might reduce the flux necessary for 7% overlap and lower the estimations to align with the expected trend. For the isobaric pair Ra^+ and Fr^+, the maximal ion flux was attained within the measured range of multiplicities, yet the maximal ion flux was estimated using the simplified model. The actual multiplicity where peak coalescence occurs can be readily determined in future studies by further analysis of the same data file.

Lastly, it would be beneficial to investigate the multiplicity distributions for more beamgate values and to extract at which the isobars become indistinguishable, since the beamgate can be controlled. On the other hand, different sources might produce ions at varying rates, meaning that the relation between beamgate and observed multiplicities depends on many more variables and differs between offline and online beams. This makes it challenging to avoid space charge

effects altogether, since a fixed beamgate might yield a low count rate with one source but already cause peak coalescence for another. It is recommended to keep the beamgate low, such that the distribution in multiplicities is small and space charge effects are minimized. A possible next step to avoid high ion loads in the MR-ToF MS is to raise and lower the cavity potential of the MR-ToF MS repeatedly at intervals such that contaminations are ejected backwards from the device. Although this method might largely reduce space charge effects in the MR-ToF MS and would contribute to the mass separation, more analysis is required to check its feasibility in the ISOLTRAP setup.

7 Conclusion

A new target holder has been designed in preparation for target identification with ISOLTRAP's recently installed laser ablation ion source. ToF spectra were obtained for CuBe, aluminium and glassy carbon samples by means of shoot-through measurements in the MR-ToF MS device. For the first two targets, poor statistics were acquired and only $Be_3{}^+$ could be properly assigned to a significant peak in the CuBe spectrum. A lower mass selection in the pulsed drift tube or a higher energy transfer from the laser may improve these spectra in future measurements. In contrast, the carbon source yielded a broad spectrum, showing peaks at each carbon cluster between $C_3{}^+$ and $C_{20}{}^+$. Many other peaks were discovered in the spectrum, representing a molecule at most mass numbers between $A = 36$ and $A = 84$. These molecules were assumed to be hydrocarbons, produced by reactions with hydrogen in the residual gas and by fragmentation due to collisions. The molecules were shown to be largely formed in the main buncher by increasing the cooling time of the bunches. The peaks corresponding to $C_{2n}H_2{}^+$, $C_{2n}H_5{}^+$ and $C_{2n+1}H^+$ appear to be preferred, though the reason for this is yet unknown. Measurements with higher revolution counts in the MR-ToF MS are to be conducted to more precisely identify the content of each molecule and to separate the broad peaks at heavier clusters.

Space charge effects in the MR-ToF MS were investigated using three isobaric pairs from the ISOLDE beam with $\Delta m/m$ ratios of 80642, 89821 and 114693. In all three cases, a linear decrease in the ToF difference was observed for a rise in ion load through the MR-ToF MS. The maximal ion fluxes at which the peaks in the spectrum become indistinguishable were estimated to be 5900 ions/s, 1600 ions/s and 700 ions/s respectively, which are higher fluxes than expected from simulations and previous experiments. This offset might be partially due to the assumption that the ToF peaks are Guassian in nature, which was made for estimating the multiplicity at which the peaks become indistinguishable. Since a single beamgate value produces a distribution of observed multiplicities, the obtained values do not establish a clear range of usable beamgates for the MR-ToF MS. Furthermore, different sources might produce ions at different rates and change the relation between beamgate and obtained multiplicities. Hence, more research is necessary on avoiding high ion loads in the MR-ToF MS. A potential solution to be investigated is to eject contaminations from the MR-ToF MS by switching the cavity voltage, allowing for better separation and a reduction of space charge effects.

References

[1] M. Mukherjee, D. Beck, K. Blaum, *et al.*, "ISOLTRAP: An on-line penning trap for mass spectrometry on short-lived nuclides," *The European Physical Journal A*, vol. 35, no. 2, pp. 1–29, 2008, ISSN: 1434-601X. DOI: https://doi.org/10.1140/epja/i2007-10528-9.

[2] C. H. Bae and S. M. Park, "A time-of-flight quadrupole mass spectrometric study of C_n^+(n=1–24) ions produced by laser ablation of a graphite target," *The Journal of Chemical Physics*, vol. 117, no. 11, pp. 5347–5353, Aug. 2002, ISSN: 0021-9606. DOI: 10.1063/1.1500356. [Online]. Available: https://doi.org/10.1063/1.1500356.

[3] K. Blaum, G. Bollen, F. Herfurth, *et al.*, "Carbon clusters for absolute mass measurements at ISOLTRAP," *The European Physical Journal A*, vol. 15, pp. 245–248, 2002, ISSN: 1387-3806. DOI: https://doi.org/10.1140/epja/i2001-10262-4.

[4] P. Fischer and L. Schweikhard, "Disentangling polycationic fullerenes produced from glassy carbon with multireflection time-of-flight mass spectrometry," *Phys. Rev. Res.*, vol. 4, p. 043 187, 4 Dec. 2022. DOI: 10.1103/PhysRevResearch.4.043187. [Online]. Available: https://link.aps.org/doi/10.1103/PhysRevResearch.4.043187.

[5] F. Maier, F. Buchinger, L. Croquette, *et al.*, "Increased beam energy as a pathway towards a highly selective and high-flux MR-ToF mass separator," *Nuclear Instruments and Methods in Physics Research Section A: Accelerators, Spectrometers, Detectors and Associated Equipment*, vol. 1056, p. 168 545, 2023, ISSN: 0168-9002. DOI: https://doi.org/10.1016/j.nima.2023.168545. [Online]. Available: https://www.sciencedirect.com/science/article/pii/S0168900223005351.

[6] G. Bollen, J. Dilling, A. M. G. Dezfuli, *et al.*, "A radio frequency quadrupole ion beam buncher for ISOLTRAP," *AIP Conference Proceedings*, vol. 455, no. 1, pp. 965–968, Dec. 1998, ISSN: 0094-243X. DOI: 10.1063/1.57380. [Online]. Available: https://doi.org/10.1063/1.57380.

[7] F. Herfurth, J. Dilling, A. Kellerbauer, *et al.*, "A linear radiofrequency ion trap for accumulation, bunching, and emittance improvement of radioactive ion beams," *Nuclear Instruments and Methods in Physics Research Section A: Accelerators, Spectrometers, Detectors and Associated Equipment*, vol. 469, no. 2, pp. 254–275, 2001, ISSN: 0168-9002. DOI: https://doi.org/10.1016/S0168-9002(01)00168-1. [Online]. Available: https://www.sciencedirect.com/science/article/pii/S0168900201001681.

[8] F. Wienholtz, S. Kreim, M. Rosenbusch, L. Schweikhard, and R. N. Wolf, "Mass-selective ion ejection from multi-reflection time-of-flight devices via a pulsed in-trap lift," *International Journal of Mass Spectrometry*, vol. 421, pp. 285–293, Oct. 2017. DOI: 10.1016/J.IJMS.2017.07.016.

[9] R. Wolf, F. Wienholtz, D. Atanasov, *et al.*, "ISOLTRAP's multi-reflection time-of-flight mass separator/spectrometer," *International Journal of Mass Spectrometry*, vol. 349-350, pp. 123–133, 2013, 100 years of Mass Spectrometry, ISSN: 1387-3806. DOI: https://doi.org/10.1016/j.ijms.2013.03.020. [Online]. Available: https://www.sciencedirect.com/science/article/pii/S1387380613001115.

[10] G. Savard, S. Becker, G. Bollen, *et al.*, "A new cooling technique for heavy ions in a Penning trap," *Physics Letters A*, vol. 158, no. 5, pp. 247–252, 1991, ISSN: 0375-9601. DOI: https://doi.org/10.1016/0375-9601(91)91008-2. [Online]. Available: https://www.sciencedirect.com/science/article/pii/0375960191910082.

[11] M. König, G. Bollen, H.-J. Kluge, T. Otto, and J. Szerypo, "Quadrupole excitation of stored ion motion at the true cyclotron frequency," *International Journal of Mass Spectrometry and Ion Processes*, vol. 142, no. 1, pp. 95–116, 1995, ISSN: 0168-1176. DOI: https://doi.org/10.1016/0168-1176(95)04146-C. [Online]. Available: https://www.sciencedirect.com/science/article/pii/016811769504146C.

[12] S. Eliseev, K. Blaum, M. Block, *et al.*, "Phase-imaging ion-cyclotron-resonance measurements for short-lived nuclides," *Phys. Rev. Lett.*, vol. 110, p. 082 501, 8 Feb. 2013. DOI: 10.1103/PhysRevLett.110.082501. [Online]. Available: https://link.aps.org/doi/10.1103/PhysRevLett.110.082501.

[13] S. Purushothaman, S. Ayet San Andrés, J. Bergmann, *et al.*, "Hyper-EMG: A new probability distribution function composed of exponentially modified gaussian distributions to analyze asymmetric peak shapes in high-resolution time-of-flight mass spectrometry," *International Journal of Mass Spectrometry*, vol. 421, pp. 245–254, 2017, ISSN: 1387-3806. DOI: https://doi.org/10.1016/j.ijms.2017.07.014. [Online]. Available: https://www.sciencedirect.com/science/article/pii/S1387380616302913.

[14] P. Bolotskikh, D. Grinfeld, A. Makarov, and M. Monastyrskiy, "Coulomb dynamics of ion bunches in multi-reflection electrostatic traps," *Nuclear Instruments and Methods in Physics Research Section A: Accelerators, Spectrometers, Detectors and Associated Equipment*, vol. 645, no. 1, pp. 146–152, 2011, The Eighth International Conference on Charged Particle Optics, ISSN: 0168-9002. DOI: https://doi.org/10.1016/j.nima.2010.12.170. [Online]. Available: https://www.sciencedirect.com/science/article/pii/S0168900210029724.

[15] J. R. Heath, Q. Zhang, S. C. O'brien, R. F. J. Curl, H. W. Kroto, and R. E. Smalley, "The formation of long carbon chain molecules during laser vaporization of graphite," *Journal of the American Chemical Society*, vol. 109, pp. 359–363, 1987. [Online]. Available: https://api.semanticscholar.org/CorpusID:97274261.

[16] M. Doverstål, B. Lindgren, U. Sassenberg, and H. Yu, "Reaction of small carbon clusters with hydrogen during laser vaporization of graphite," *Zeitschrift für Physik D Atoms, Molecules and Clusters*, vol. 19, pp. 447–449, 4 1991. DOI: 10.1007/BF01448349. [Online]. Available: https://doi.org/10.1007/BF01448349.

[17] M. Au, M. Athanasakis-Kaklamanakis, L. Nies, *et al.*, "In-source and in-trap formation of molecular ions in the actinide mass range at CERN-ISOLDE," *Nuclear Instruments and Methods in Physics Research Section B: Beam Interactions with Materials and Atoms*, vol. 541, pp. 375–379, 2023, ISSN: 0168-583X. DOI: https://doi.org/10.1016/j.nimb.2023.05.015. [Online]. Available: https://www.sciencedirect.com/science/article/pii/S0168583X23002112.